Title
Diverse wave-particle interactions for energetic ions that traverse Alfvén eigenmodes on their first full orbit

Journal
Physics of Plasmas, 23(2)

ISSN
1070-664X

Authors
Heidbrink, WW
Persico, EAD
Austin, ME
et al.

Publication Date
2016-02-01

DOI
10.1063/1.4941587

Diverse wave-particle interactions for energetic ions that traverse Alfvén eigenmodes on their first full orbit

W. W. Heidbrink,[1] E. A. D. Persico,[1] M. E. Austin,[2] Xi Chen,[3] D. C. Pace,[3] and M. A. Van Zeeland[3]
[1]*University of California Irvine, Irvine, California 92697, USA*
[2]*University of Texas, Austin, Texas 78705, USA*
[3]*General Atomics, San Diego, California 92186, USA*

(Received 3 October 2015; accepted 22 January 2016; published online 9 February 2016)

Neutral-beam ions that are deflected onto loss orbits by Alfvén eigenmodes (AE) on their first bounce orbit and are detected by a fast-ion loss detector (FILD) satisfy the "local resonance" condition proposed by Zhang *et al.* [Nucl. Fusion **55**, 22002 (2015)]. This theory qualitatively explains FILD observations for a wide variety of AE-particle interactions. When coherent losses are measured for multiple AE, oscillations at the sum and difference frequencies of the independent modes are often observed in the loss signal. The amplitudes of the sum and difference peaks correlate weakly with the amplitudes of the fundamental loss-signal amplitudes but do not correlate with the measured mode amplitudes. In contrast to a simple uniform-plasma theory of the interaction [Chen *et al.*, Nucl. Fusion **54**, 083005 (2014)], the loss-signal amplitude at the sum frequency is often larger than the loss-signal amplitude at the difference frequency, indicating a more detailed computation of the orbital trajectories through the mode eigenfunctions is needed.
[http://dx.doi.org/10.1063/1.4941587]

I. INTRODUCTION

Neutral-beam ions that are deflected into a loss detector on their first bounce orbit act like a "light-ion beam probe" that detects wave-particle interactions between fast ions and Alfvén eigenmodes (AE).[1] Although other neutral beams generally inject and help to drive the AE instabilities, the plasma conditions are arranged so that one particular source acts as the dominant source of signal at the fast-ion loss detector (FILD). Experimentally, this is achieved by adjusting the plasma current so that source neutrals that ionize near the last-closed flux surface (LCFS) execute an orbit that brings them near the loss detector on their first bounce orbit. Since the first orbit is primarily determined by the equilibrium fields, the geometry and duration of the wave-particle interaction are well-known. This is in contrast to most measurements of fast ions expelled by AE (e.g., Ref. 2), where the lost ions typically interact with the wave for many orbital cycles. In the light-ion beam probe configuration, the amplitude of the fluctuating signal measured by the loss detector at mode frequencies is proportional to the neutral-beam ionization gradient.[1,3] Because the beam-deposition profile is known accurately, the loss-detector fluctuation measurements yield a direct measurement of the orbital displacement by the AEs. The inferred displacement in a single bounce orbit through a mode is often quite large,[3,4] $\sim 10 \pm 2$ cm.

In a recent paper,[5] Zhang *et al.* argue that large displacements occur when the ion stays in phase with the wave as it traverses the AE. Under normal circumstances, large displacements only occur when particles stay in phase with the wave for many orbital cycles. For a mode with a frequency ω that is much less than the cyclotron frequency, the usual resonance condition is

$$\omega = n\omega_\phi - (m + l)\omega_\theta, \tag{1}$$

where ω_ϕ and ω_θ are the toroidal and poloidal orbital frequencies, n and m are the toroidal and poloidal mode numbers, and l is an integer. However, in a single pass through a spatially localized mode, the requirement that the ion stays in phase with the wave takes on a different form

$$\omega = n\langle\dot{\phi}\rangle - m\langle\dot{\theta}\rangle. \tag{2}$$

Here, $\langle\dot{\phi}\rangle$ and $\langle\dot{\theta}\rangle$ are the average toroidal and poloidal angular velocities during the portion of the orbit that traverses the mode. Because the orbit is large and the Alfvén eigenmode is of limited spatial extent, $\langle\dot{\phi}\rangle$ and $\langle\dot{\theta}\rangle$ differ considerably from the customary (orbit-averaged) precession and bounce frequencies ω_ϕ and ω_θ; in fact, for the conditions of our DIII-D experiment, $\langle\dot{\phi}\rangle$ and ω_ϕ are in opposite directions. A recent paper[6] argues that resonant interactions of this type could influence AE stability.

In addition to fluctuations at AE frequencies, the FILD signal contains information about nonlinear interactions between the ions and the waves.[7] In particular, in the presence of two AEs with frequencies f_1 and f_2, the FILD signals oscillate at the sum frequency $f_1 + f_2$, at the difference frequency $|f_1 - f_2|$, and at second harmonic frequencies, $2f_1$ and $2f_2$. Reference 7 contains a simple calculation that shows that, in a uniform plasma, orbital deflections by two modes will produce signal oscillations at the sum and difference frequencies. The calculation predicts a larger amplitude at the difference frequency than at the sum frequency, consistent with the experimental example shown in Ref. 7.

In this paper, the generality of the results shown in Ref. 7 is checked against a larger set of data. We find that although many examples like the one shown in Ref. 7 exist, there are many exceptions. In particular, the amplitude of

oscillations at the sum frequency often exceeds the amplitude of oscillations at the difference frequency; also, spectral peaks at the second harmonic are often absent. Second, this paper compares the "local resonance" condition given by Eq. (2) with experiment. We find that the theory of Ref. 5 successfully explains multiple features of the data.

The paper begins with a description of the apparatus (Sec. II). Next, representative examples of the wide variety of FILD spectra are shown and interpreted (Sec. III). Conclusions follow in Sec. IV.

II. APPARATUS AND ANALYSIS PROCEDURE

The experiment is performed during the current ramp on the DIII-D tokamak (major radius $R \simeq 1.7$ m, minor radius $a \simeq 0.6$ m). The probing particles are 81 keV deuterons from a neutral beam that injects in the midplane in the direction of the plasma current at a tangency radius of $R_{tan} = 1.15$ m. Typically, the toroidal field is 2.0 T, the plasma current is 0.8 MA, and the q profile is reversed with $q_{min} \simeq 4$. The line-average electron density, central electron temperature, and central ion temperature are approximately $\bar{n}_e = 2.0 \times 10^{19}$ m^{-3}, $T_e(0) = 3.8$ keV, and $T_i(0) = 1.5$ keV. The plasma is an oval shape that is limited on the carbon inner wall (Fig. 1).

The primary diagnostic for the experiment is a scintillator-based FILD[8] that is mounted close to the midplane[9] (Fig. 1). Some of the light from the scintillator is imaged onto a CCD camera in order to provide detailed information about the pitch and gyroradius of the lost ions; photomultipliers (PMT) measure light from portions of the scintillator for high temporal-resolution measurements. The data in this paper are from a PMT that measures the "prompt-loss" spot shown in Fig. 2. In this figure, the measured equilibrium has been used to map the actual scintillator image into energy and pitch coordinates. Within experimental accuracy, which is ~5° for pitch angle but poor for energy,[10] the primary spot on the scintillator is from prompt losses of the probing beam. To check that the PMT signal is dominated by first-orbit losses, one or more "notches" are programmed in the beam waveform (Fig. 3(a)). For all discharges included in this study, the PMT signal drops to approximately zero within ~100 μs of the beam notch (Fig. 3(b)), which is the timescale of a single bounce period. The FILD diagnostic is not absolutely calibrated but the data analyzed here are all from the same week of operation, so relative amplitude comparisons are meaningful.

As is typical for DIII-D studies of AEs during the current ramp,[11] neutral-beam heating excites both reversed-shear AEs (RSAE) and toroidal AEs (TAE). Global measurements of internal AE activity are detected using CO_2 interferometry[12] along the four chords illustrated in Fig. 1. Radial profiles are measured by a 40-channel electron cyclotron emission (ECE) radiometer diagnostic.[13] Toroidal mode numbers are measured by a toroidal array of Mirnov coils at the outer midplane.[14]

A database is constructed from 48 discharges acquired during two days of dedicated experiments. The requirement that first-orbit losses dominate the FILD signal excludes six shots. Next, the FILD PMT data are Fourier analyzed. The

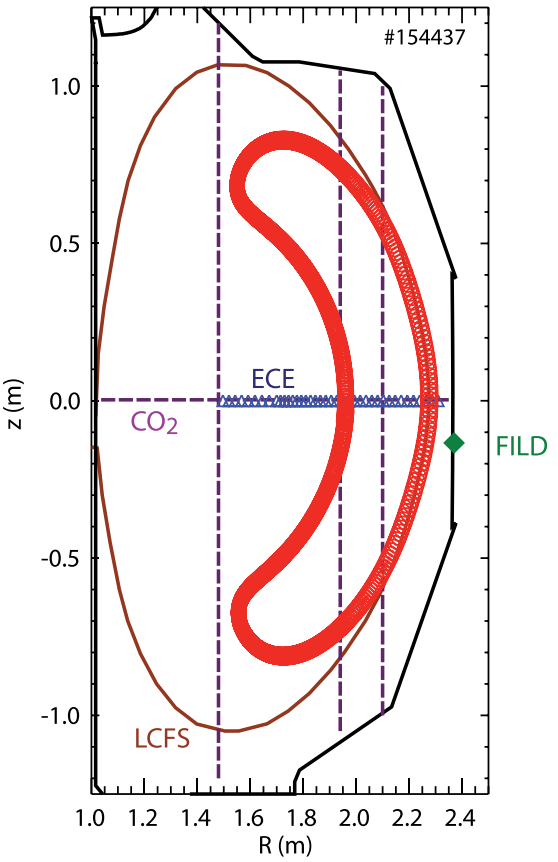

FIG. 1. Elevation of DIII-D showing the vacuum vessel, last closed flux surface, the interferometer chords (dashed lines), position of the ECE radiometer channels (△), and location of the FILD detector (◇). A projection of the orbit in the equilibrium field represented by the asterisk in Fig. 7 is also shown.

time histories of the FILD spectra are examined for coherent peaks that persist across more than 5 ms without changing in frequency faster than ~1 kHz/ms. To reduce complexity, we select times with less than four significant peaks in the RSAE and TAE frequency range. This yields 23 shot and time combinations to consider further. Figure 4 shows an example of a FILD spectrum that satisfies these criteria

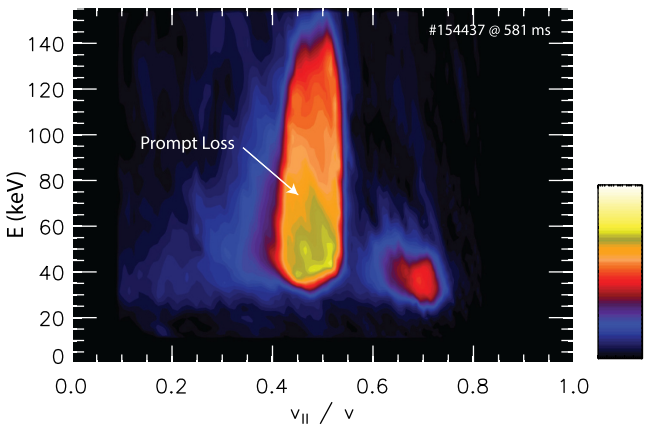

FIG. 2. FILD scintillator image mapped onto a (pitch, energy) grid near the time of the FILD spectrum in Fig. 4. The prompt-loss peak produced by the probe beam is indicated. A linear scale rainbow contour map is employed.

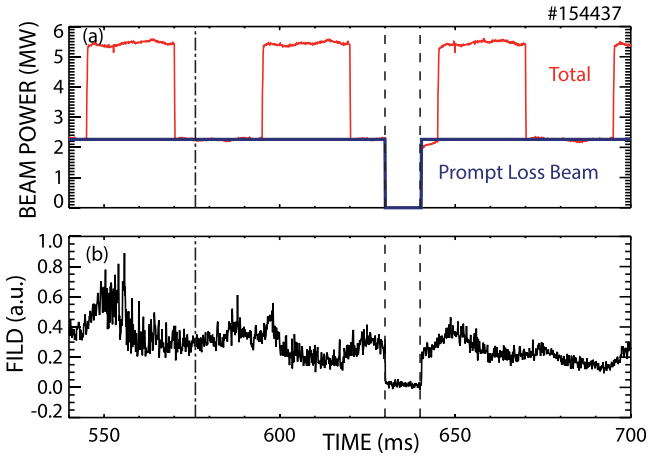

FIG. 3. (a) Total beam power and power injected by the probe beam vs. time. (b) FILD PMT signal vs. time. The FILD signal drops to approximately zero at the time of the beam notch (dashed lines). The time of the spectrum shown in Fig. 4 is indicated by the dashed-dotted line.

for two "fundamental" frequencies, one at ∼93 kHz and the other at ∼101 kHz.

Analysis continues with the 40-channel ECE data (Fig. 5). A program finds the channel with the strongest signal for each of the FILD fundamental frequencies. To reduce noise, the signal from this selected channel is averaged with the two adjacent channels over three time steps, centered at the time of interest. This averages nine spectra together. The resulting ECE spectrum for the 101 kHz mode of Fig. 4 appears in Fig. 5(b). A Gaussian is fit to the peak. The center of the Gaussian is stored in the database as the fundamental frequency. Additionally, a Gaussian fit is performed to the radial profile of the mode (Fig. 5(c)). The center of the Gaussian is saved as the radial center, and the full-width quarter-max of the Gaussian is saved as the minimum and maximum radii R_{min} and R_{max} of the mode.

Next, with the fundamental frequencies determined, the FILD spectrum is reanalyzed to find the amplitude of the peaks at the fundamental, sum, difference, and second-harmonic frequencies.

For a subset of the modes, analysis of the magnetics data yields the toroidal mode number. Figure 6 shows unambiguous

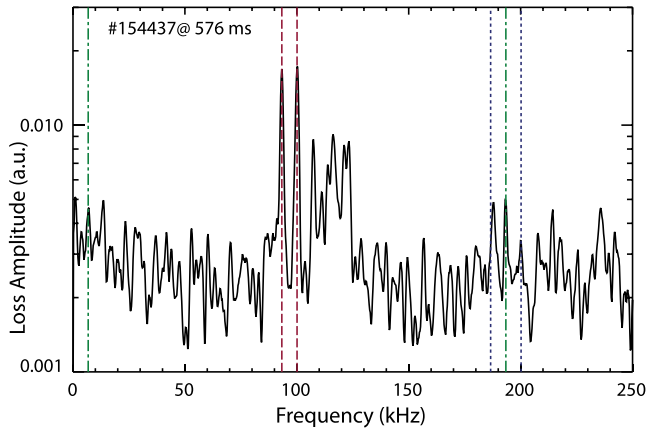

FIG. 4. FILD amplitude spectrum. The fundamental peaks are marked by the long-dashed lines, the second harmonic peaks by the short-dashed lines, and the sum and difference peaks by the dotted-dashed lines.

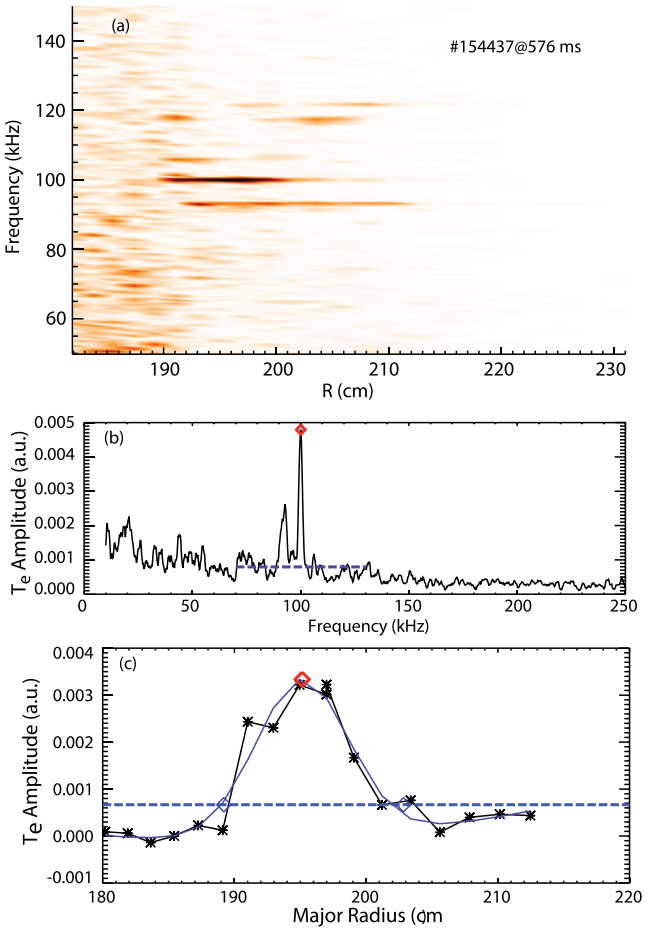

FIG. 5. ECE data for the case in Fig. 4. (a) Overview of the data from all 40 channels at a single time slice. (b) Spectrum after processing to select channels at the radial peak for the 101 kHz mode. The peak amplitude entered in the database is the difference between the diamond and the background estimate (dashed line). (c) Radial profile for the 101 kHz mode. The radial position of the peak is indicated by the diamond; the dashed line indicates the quarter-maximum selected to measure the radial extent of the mode.

fits of $n = 2$ and $n = 3$ for the two fundamental peaks of Fig. 4. Definitive identification of the toroidal mode number is impossible for approximately half of the selected modes.

III. RESULTS

Zhang *et al.*[5] predict that large displacements occur when Eq. (2) is satisfied. If their prediction is correct, large peaks in the FILD spectrum should occur when the following four conditions are satisfied:

(1) Orbits exist that satisfy Eq. (2).
(2) The potentially resonant orbits actually intersect the mode spatially.
(3) The orbit passes close to the FILD detector.
(4) The probe beam populates these resonant orbits.

To check this prediction, we compute guiding-center orbits for the case shown in Fig. 4. The equilibrium reconstructed by the EFIT code[15] using motional Stark effect[16] and magnetics data has a reversed q profile that is consistent with the observed RSAE activity and preserves T_e as a flux function. Figure 7 classifies the possible orbits within topological boundaries in terms of the magnetic moment μ and the

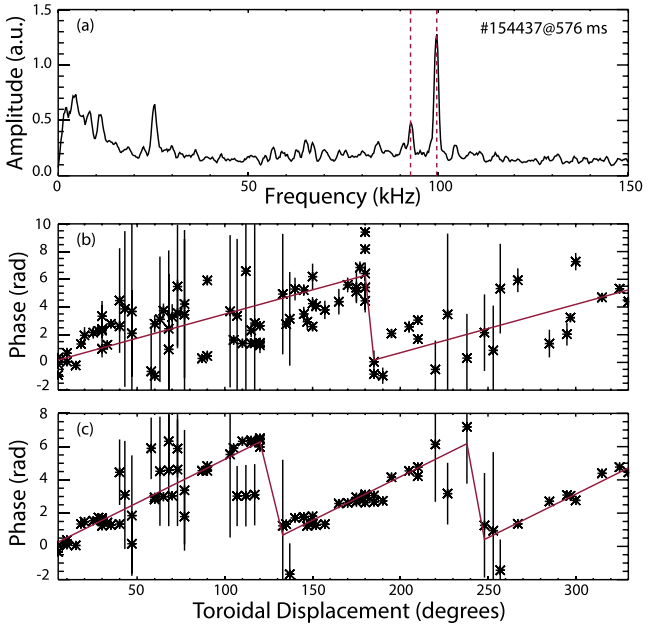

FIG. 6. Magnetics data for the case in Fig. 4. (a) Average spectrum for the toroidal array. ((b) and (c)) Phase difference between all possible probe pairs vs. toroidal displacement for the (b) $n=2$ 93 kHz mode and the (c) $n=3$ 101 kHz mode. The error bars are derived from the coherence.

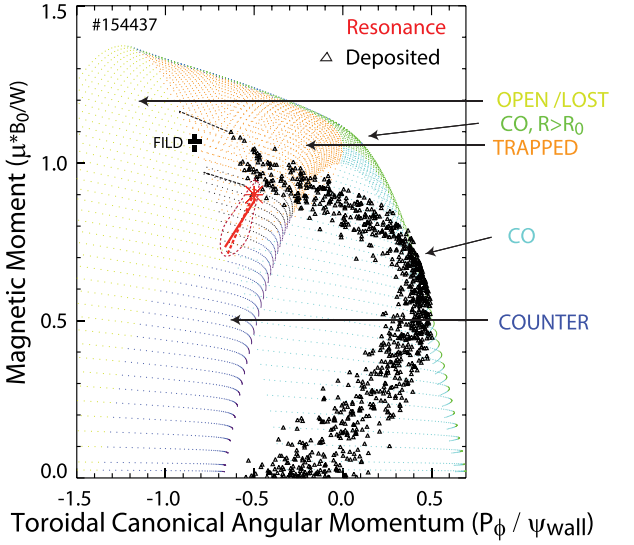

FIG. 7. Orbit topology map for the case of Fig. 4. The abscissa is the toroidal canonical angular momentum normalized to the poloidal flux at the last-closed flux surface. The ordinate is the magnetic moment normalized by the particle energy and magnetic field at the magnetic axis. A fit to the equilibrium orbits that satisfy the resonance condition (Eq. (2)) for the 93 kHz mode, intersect the mode, and approach the FILD is indicated by the solid line; a similar fit for resonant orbits for the 101 kHz mode is indicated by the dashed line; the dotted line encircles the portion of phase space occupied by resonant orbits. The resonant orbit plotted in Fig. 1 is marked by the asterisk. The small triangles represent orbits that are populated by the injected neutral beams; neutrals that ionize in the scrapeoff plasma appear between the dashed lines to the left of the triangles. The large + represents the location of the FILD prompt loss spot (Fig. 2) in constants-of-motion space. The various orbit types listed in the legend are lost orbits (including orbits on open field lines), co-passing orbits that do not encircle the magnetic axis, trapped orbits, axis-encircling co-passing orbits, and counter-passing orbits.

toroidal canonical angular momentum P_ϕ. Trapped particles are the relevant orbits. To estimate $\langle\dot{\phi}\rangle$ and $\langle\dot{\theta}\rangle$ in Eq. (2), we compute $\dot{\phi}$ and $\dot{\theta}$ when the ion crosses the midplane on the inner leg of the banana orbit. The poloidal mode number is approximated as $m=nq$. Since the calculated resonance width in Ref. 5 is broad ($\delta\omega/\omega_\theta\sim 6$), orbits that satisfy the resonance condition to within $\delta\omega/\omega<20\%$ are retained as orbits that satisfy condition #1. To satisfy condition #2, only orbits that traverse the midplane between R_{min} and R_{max} as inferred from the ECE data are retained. To satisfy condition #3, the guiding-center orbit must extend beyond $R=2.23$ m. Orbits that simultaneously satisfy these three conditions for the 93 and 101 kHz modes are indicated by the solid and dashed lines in Fig. 7. To check the fourth condition, the beam deposition is calculated for the measured density, temperature, and Z_{eff} profiles. Deposited orbits are indicated by triangles in Fig. 7. Since profile data are unavailable outside the LCFS in this discharge, the calculated deposition neglects ionization in this region but, in reality, some orbits are populated in the scrapeoff region, which is to the left of the populated orbits in the figure. It is evident from the intersection of the resonance curve and the deposition pattern that all four criteria are satisfied in this discharge for both of the observed FILD peaks, as predicted by Zhang's theory.

An orbit that satisfies resonant conditions with both modes and originates at the plasma edge is marked with an * in Fig. 7. A projection of this orbit is plotted in Fig. 1. The pitch of this orbit at the plasma edge is consistent with the measured FILD camera image (Fig. 2). The equilibrium orbits that satisfy a resonance condition span a substantial range in parameters: pitch by FILD of 0.4–0.66, minimum guiding center radius of $\rho=0.32$–0.47, maximum guiding center radius of $\rho=0.90$–1.13, toroidal velocity on the inner leg of the banana of 0.9–1.6×10^6 m/s, and vertical velocity on the inner leg of the banana of 1.0–1.7×10^5 m/s. (Here, the minor radius variable is ρ, the normalized square root of the toroidal flux.)

Unstable modes are often observed that do not produce peaks in the FILD spectra. One reason this occurs is failure to satisfy condition #2, i.e., the orbit does not intersect the mode. This often happens late in the current ramp, when the orbital banana width has shrunk and the q_{min} surface has contracted toward the magnetic axis. Data showing the importance of this effect was already published in Fig. 6 of Ref. 4.

This effect does not account for all of the cases of unstable modes that do not appear in the FILD spectra, however. Figure 8 shows an example of a weak FILD signal because conditions #1 and #4 are not satisfied simultaneously. A strong mode at 73.5 kHz is observed on the ECE (Fig. 8(a)) but is barely visible in the FILD spectrum (Fig. 8(b)). Figure 8(c) repeats the analysis of Fig. 7 for this discharge. The resonance condition for this $n=3$ mode is satisfied in a portion of phase space that is hardly populated by the probing beam.

There are also many examples of FILD peaks that do *not* correspond to a mode observed by the ECE. For the FILD spectrum shown in Fig. 9, only the peaks at 80.6, 87.9, and 93.3 kHz (labeled 1, 2, and 3 in the figure) are prominent in the ECE data. However, many other peaks in the FILD spectrum correspond with modes that are only detected by the two outermost interferometer chords (peaks labeled 4–9 in the figure). This is true for the vast majority of FILD peaks

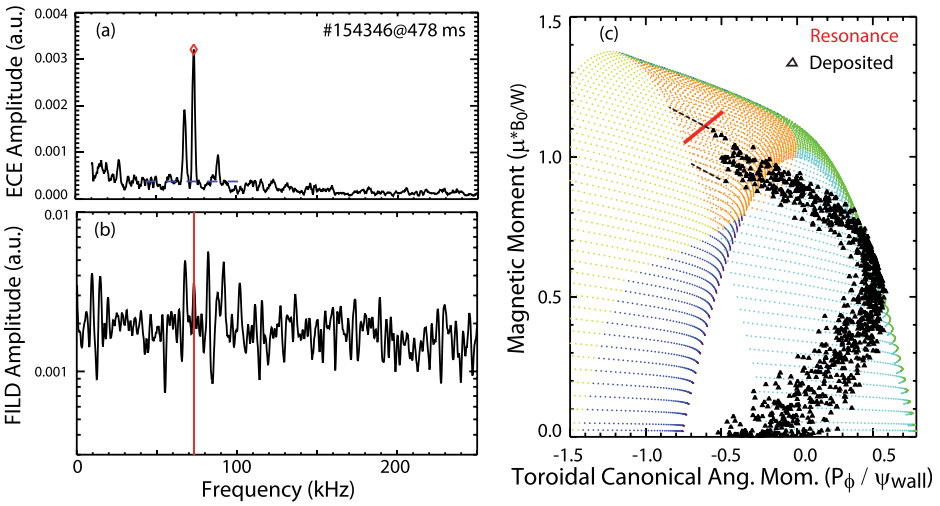

FIG. 8. (a) ECE and (b) FILD frequency spectra for a strong mode in the ECE that appears weakly in the FILD signal. (c) Resonance map (cf. Fig. 7) for this case. The orbits that satisfy the resonance condition (solid line) hardly overlap with the deposited orbits (small triangles).

that are not detected by ECE: Most of these modes are visible on an interferometer channel, usually one of the two outer channels. Only a handful of FILD peaks are absent in all ECE, interferometer, and Mirnov signals. The weak relationship between the ECE amplitude and the FILD amplitude is confirmed by examination of the database; these two amplitudes are basically uncorrelated (correlation coefficient $r = 0.15$).

The midplane FILD measures losses at a fixed location on the wall (Fig. 1). In principle, modes that appear on the fluctuation diagnostics could be absent in the FILD spectra because expelled ions strike other locations, such as the vacuum vessel floor; however, for the class of orbits that are the focus of this study, calculations[3,5] predict losses concentrated near the midplane. Past experimental results[17] also show that AE-induced losses are usually concentrated near the midplane.

Turning to nonlinear effects, two or more peaks in the FILD spectrum at fundamental frequencies often generate peaks at sum and difference frequencies. (In contrast, peaks at sum and difference frequencies are *not* observed for the modes themselves on any fluctuation diagnostic.[7]) For example, for the relatively simple case of two fundamental peaks at $f_1 \simeq 93$ and $f_2 \simeq 101$ kHz shown in Fig. 4, peaks occur at $f_1 + f_2 \simeq 194$ kHz and $f_2 - f_1 \simeq 8$ kHz. For the complicated case shown in Fig. 9, identifiable peaks occur at most of the sum frequencies and for some of the difference frequencies. Restricting the database to simple cases with fewer than four fundamental peaks, the magnitude of the sum and difference peaks tend to scale with the product of the amplitude of the fundamental FILD peaks (Fig. 10). For this dataset, the correlation coefficient of the difference (sum) amplitude with the fundamental product is $r = 0.90$ (0.59). In contrast, the product of fundamental ECE amplitudes is uncorrelated with the magnitudes of the FILD difference and sum amplitudes, which is expected since the fundamental amplitudes are also uncorrelated.

The analytical theory of Ref. 7 predicts that the amplitude of the difference peak should exceed the amplitude of the sum peak by the ratio $(f_1 + f_2)^2/(f_1 - f_2)^2$. Although the amplitude of the difference peak is larger than the sum peak for the example in Ref. 7, examination of our larger dataset shows that this is not generally the case. In particular, the sum peak is larger than the difference peak in Fig. 4, for

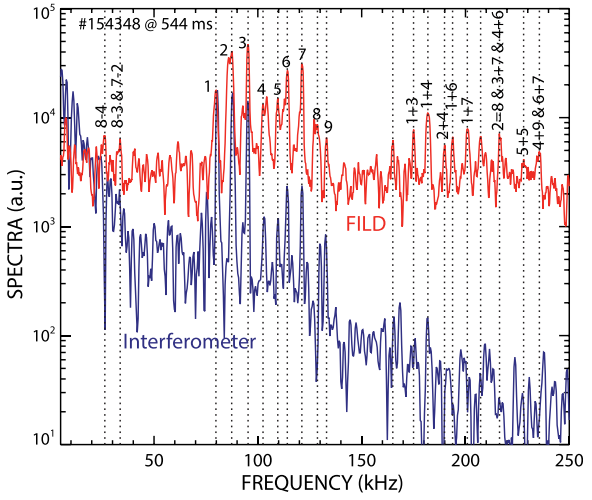

FIG. 9. FILD amplitude spectrum and CO_2 interferometer cross-power spectrum between the two outermost vertical chords for a case with many peaks in the FILD spectrum. The fundamental frequencies are marked by numbers between 1 and 9. The sum, difference, and second-harmonic peaks are identified by the numbers of the fundamental modes that produce that feature.

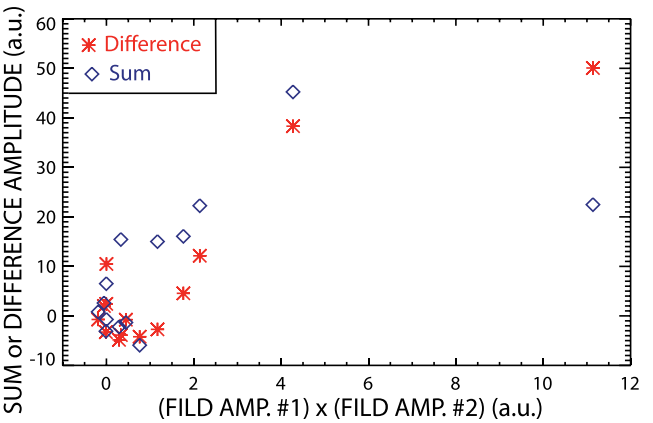

FIG. 10. Amplitude of FILD sum (◇) and difference (*) peaks vs. the product of the amplitudes of the two fundamental peaks for all of the "simple" cases with less than four fundamental FILD peaks in the spectrum.

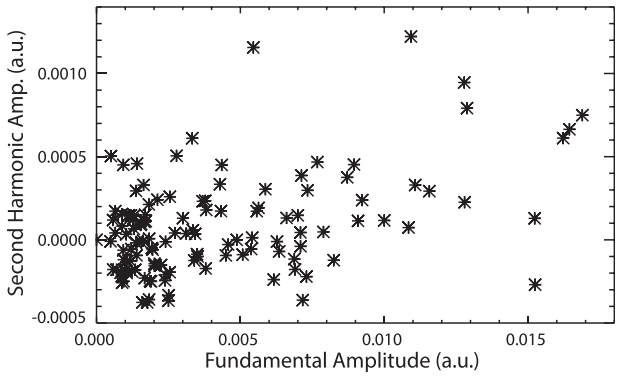

FIG. 11. Amplitude of FILD second harmonic peaks vs. the fundamental peaks for all of the modes in the database.

most of the peaks in Fig. 9, and for many of the shots in Fig. 10. Evidently, the uniform plasma model that yields Eq. (4) of Ref. 7 is too simplistic to account for the wide variety of wave-particle interactions that occur when probing ions traverse the actual, spatially localized modes.

The simple analytical theory predicts a peak at the second harmonic of the fundamental that scales with the square of the fundamental amplitude. Once again, reality is more complicated. There is only a weak correlation of second harmonic amplitude with fundamental amplitude (Fig. 11) ($r = 0.45$). Indeed, examination of the individual cases shown in Figs. 4 and 9 shows that the correlation of the second harmonic amplitude with the primary amplitude is weak.

IV. DISCUSSION

This work has two major findings. The first finding is that the conceptual picture proposed in Ref. 5 is a powerful organizing principle. At first blush, the FILD data are mystifying, with peaks seemingly randomly appearing with little relationship to the observed modes. However, the four criteria listed in Sec. III can account for virtually every observation. For a fundamental peak to be observed, the resonance condition (Eq. (2)) must be satisfied on a portion of the orbit. This quantitatively explains the observation of both peaks in the case of Fig. 4 and the absence of a peak in the case of Fig. 8. Presumably, for the peaks that correspond to modes only detected by interferometer channels (Fig. 9), a similar resonant wave-particle interaction takes place somewhere along the orbital path. When modes are observed on the fluctuation diagnostics but not by FILD, the probing orbits either fail to stay in phase with the mode (Eq. (2)) or fail to traverse the mode eigenfunction (Fig. 6 of Ref. 4).

The second major finding concerns the nonlinear interactions. Reference 7 argues that nonlinearities occur because the radial displacement δr imparted by the first mode alters the phase the particle experiences when it interacts with the second mode (through the $\mathbf{k} \cdot \mathbf{r}$ term that appears in the particle phase). This part of the argument in Ref. 7 is almost certainly correct. When two peaks occur in the FILD spectrum, because of the relatively stringent conditions required to observe a peak, both peaks are usually produced by the same set of orbits. If one mode causes a large orbital displacement, it inevitably affects the particle phase at the second mode. This explains why the majority of strong primary peaks produce a nonlinear feature in the spectrum (e.g., Fig. 9) and also explains why there is a correlation between the product of the fundamental amplitudes and the sum and difference amplitudes (Fig. 10). On the other hand, the actual interaction depends in a complicated manner on the orbital trajectories through the mode eigenfunctions. In light of this complexity, it is no surprise that the predictions of a simple uniform-plasma calculation only weakly correspond with the observed scalings of the second-harmonic, difference, and sum amplitudes with mode frequency and amplitude. Detailed modeling of actual cases that takes into account the full spatial complexity is required to reproduce these features. This, however, is left for future work.

ACKNOWLEDGMENTS

The assistance of the DIII-D team is gratefully acknowledged. This material was based upon work supported by the U.S. Department of Energy, Office of Science, Office of Fusion Energy Sciences, using the DIII-D National Fusion Facility, a DOE Office of Science user facility, under Award Nos. SC-G903402, DE-FC02-04ER54698, and DE-FG03-97ER54415. DIII-D data shown in this paper can be obtained in digital format by following the links at https://fusion.gat.com/global/D3D_DMP.

[1]X. Chen, W. W. Heidbrink, M. A. Van Zeeland, G. J. Kramer, D. C. Pace, C. C. Petty, M. E. Austin, R. K. Fisher, J. M. Hanson, R. Nazikian, and L. Zeng, Rev. Sci. Instrum. **85**, 11E701 (2014).
[2]M. García-Muñoz, H.-U. Fahrbach, S. Günter *et al.*, Phys. Rev. Lett. **100**, 055005 (2008).
[3]X. Chen, W. W. Heidbrink, G. J. Kramer, M. A. Van Zeeland, M. E. Austin, R. K. Fisher, R. Nazikian, D. C. Pace, and C. C. Petty, Nucl. Fusion **53**, 123019 (2013).
[4]X. Chen, M. E. Austin, R. K. Fisher, W. W. Heidbrink, G. J. Kramer, R. Nazikian, D. C. Pace, C. C. Petty, and M. A. Van Zeeland, Phys. Rev. Lett. **110**, 065004 (2013).
[5]R. B. Zhang, G. Y. Fu, R. B. White, and X. G. Wang, Nucl. Fusion **55**, 22002 (2015).
[6]W. W. Heidbrink, G. Y. Fu, and M. A. Van Zeeland, Phys. Plasmas **22**, 082507 (2015).
[7]X. Chen, G. J. Kramer, W. W. Heidbrink, R. K. Fisher, D. C. Pace, C. C. Petty, M. Podesta, and M. A. Van Zeeland, Nucl. Fusion **54**, 083005 (2014).
[8]S. J. Zweben, Nucl. Fusion **29**, 825 (1989).
[9]X. Chen, R. K. Fisher, D. C. Pace, M. García-Munoz, J. A. Chavez, W. W. Heidbrink, and M. A. Van Zeeland, Rev. Sci. Instrum. **83**, 10D707 (2012).
[10]D. C. Pace, R. Pipes, R. K. Fisher, and M. A. Van Zeeland, Rev. Sci. Instrum. **85**, 11D841 (2014).
[11]M. A. Van Zeeland, G. J. Kramer, M. E. Austin, R. L. Boivin, W. W. Heidbrink *et al.*, Phys. Rev. Lett. **97**, 135001 (2006).
[12]M. A. Van Zeeland, G. J. Kramer, R. Nazikian, H. L. Berk, T. N. Carlstrom, and W. M. Solomon, Plasma Phys. Controlled Fusion **47**, L31 (2005).
[13]M. E. Austin and J. Lohr, Rev. Sci. Instrum. **74**, 1457 (2003).
[14]E. J. Strait, Rev. Sci. Instrum. **77**, 023502 (2006).
[15]L. L. Lao, H. St. John, R. D. Stambaugh, A. G. Kellman, and W. Pfeiffer, Nucl. Fusion **25**, 1611 (1985).
[16]B. W. Rice, D. G. Nilson, and D. Wroblewski, Rev. Sci. Instrum. **66**, 373 (1995).
[17]H. H. Duong, W. W. Heidbrink, E. J. Strait, T. W. Petrie, R. Lee, R. A. Moyer, and J. G. Watkins, Nucl. Fusion **33**, 749 (1993).